Light Higgs ($H \to b\bar{b}$) at the LHC

by Andrew John Lowe

Department of Physics
Royal Holloway and Bedford New College
University of London

August 2001

CERN-THESIS-2009-050
01/11/2001

This thesis is submitted in partial fulfillment of the requirement for the degree of MSc from the University of London.

Abstract

The aim of this study was to examine the search potential of $WH(H \rightarrow b\bar{b})$ for a light Higgs boson. A cursory overview of the Standard Model of particle physics is given, followed by an introduction to some of the physical quantities that are measured in particle physics experiments. Basic theoretical concepts are discussed, and the Higgs mechanism is described. The associated production process WH is reviewed. This study is the first analysis of this type to be performed in C++ using the Atlfast-Athena detector simulator, and involved replicating the results published earlier in the ATLAS Technical Design Report. The results broadly agree with those in the published report. Based on the subset of the backgrounds to the signal that were successfully generated, a signal significance close to, but not exceeding, 5σ is achievable after three years initial operation at low luminosity.

Contents

List of Figures

List of Tables

Acknowledgements

I wish to express my gratitude to Dr Hywel Phillips, Dr Elena Brambilla, and Graham Hollyman for their invaluable help and guidance which made this thesis possible. I would also like to thank the whole Royal Holloway Particle Physics Group for their support.

Chapter 1

The Standard Model

1.1 Introduction

Particle physics is the study of subatomic particles and the fundamental forces that act between them. The current theoretical description of particle physics phenomena is known as the *Standard Model* [1, 2, 3]. In the Standard Model the fundamental particles of matter are quarks and leptons, which are fermions. Fermions are particles with half-integer spin that obey Fermi-Dirac statistics, which require that two or more identical particles cannot occupy the same quantum state simultaneously.

Quarks

There are six known types, or *flavours*, of quarks. The quarks are organised in three families, or *generations*, as shown in table 1.1 [4]. Quarks are always bound together in groups of three, called *baryons*, or in quark-antiquark pairs, called *mesons*. Isolated free quarks are not observed in nature. Baryons and mesons are collectively known as *hadrons*. Examples of baryons are the ubiquitous proton and neutron of ordinary matter.

Quarks possess an attribute whimsically called *colour*, which has no relation to colour in the everyday sense of the word. There are three quark colours:

Table 1.1: Quarks and their properties [4].

	Name	Symbol	Charge (/e)	Mass ($\times c^2$)
1^{st}	Up	u	$\frac{2}{3}$	1 to 5 MeV
generation	Down	d	-$\frac{1}{3}$	3 to 9 MeV
2^{nd}	Charm	c	$\frac{2}{3}$	1.15 to 1.35 GeV
generation	Strange	s	-$\frac{1}{3}$	75 to 170 MeV
3^{rd}	Top	t	$\frac{2}{3}$	174.3±5.1 GeV
generation	Bottom	b	-$\frac{1}{3}$	4.0 to 4.4 GeV

red (R), green (G), and blue (B). Antiquarks carry the complementary colours: antired ($\overline{\text{R}}$), antigreen ($\overline{\text{G}}$), and antiblue ($\overline{\text{B}}$). All quark bound states are colourless. A phenomenon known as *colour confinement* exists which requires that hadrons can only exist as colour-neutral states. Therefore free quarks are prohibited.

There are three possible ways of constructing colourless bound states from coloured quarks. Firstly, a red, green, and blue quark can form a baryon. Secondly, an antired, antigreen, and antiblue antiquark can form an antibaryon. Finally, a quark with any colour and an antiquark with the complementary colour can form a colourless bound state. Mesons are $q\overline{q}$ states; although $R\overline{R}$, $G\overline{G}$, and $B\overline{B}$ are colourless, it is in fact only the combination of these, $R\overline{R}+G\overline{G}+B\overline{B}$, that is observed in nature. Because the quarks within baryons are coloured differently states are allowed to exist, such as the Ω^- (= sss) or the Δ^{++} (= uuu), that would otherwise be forbidden by the rules of Fermi-Dirac statistics. These quarks are the basic components of hadrons and are known as *valence* quarks. Instead of empty space, they are surrounded by a foaming sea of virtual quark-antiquark pairs of different flavours that spontaneously pop into and out of existence.

This description of hadron substructure is, however, rather naive. Hadron substructure is more properly described by the mathematical machinery of *Quantum*

Chromodynamics (QCD), which will be discussed later.

Leptons

There are six known types of leptons. Like quarks, these are also organised in three families, as shown in table 1.2 [4]. The muon and tau can be thought of as heavier versions of the electron, which is the most familiar example of a lepton.

Table 1.2: Leptons and their properties [4].

	Name	Symbol	Charge (/e)	Mass ($\times c^2$)
1^{st}	Electron	e^-	-1	0.511 MeV
generation	Electron neutrino	ν_e	0	< 3 eV
2^{nd}	Muon	μ^-	-1	105.7 MeV
generation	Muon neutrino	ν_μ	0	< 0.19 MeV
3^{rd}	Tau	τ^-	-1	1777 MeV
generation	Tau neutrino	ν_τ	0	< 18.2 MeV

Neutrinos are weakly interacting neutral particles that travel essentially at the speed of light [5]. There is strong evidence, namely, from studies of Z^0 production in e^+e^- collisions at the Large Electron-Positron collider (LEP) [4], that only three *light* neutrino types exist. Light neutrinos are those with mass less than half the Z^0 mass. The Z^0 is a particle that will be encountered again later.

Neutrinos are assumed to be massless in the simplest version of the Standard Model, but there is no fundamental reason why this should be. If neutrinos have non-zero masses their flavour eigenstates do not have to coincide with their mass eigenstates. Consequently, a new phenomenon can occur: *neutrino oscillations*. Several experiments have been built to look for evidence of neutrino oscillations. Recent results from these experiments indicate that neutrinos do indeed possess a small, but nevertheless non-zero, mass [6].

Gauge bosons

There are four fundamental forces of nature: the electromagnetic interaction, the weak interaction, the strong interaction, and gravity. The latter of these, gravity, is neglected in the Standard Model because the gravitational force between elementary particles is extremely weak compared to the other three forces.

The fundamental forces arise from the exchange of *gauge bosons* between the fermions. For this reason they are called *exchange forces*. The gauge bosons act as force carriers. Bosons are particles with zero or integer spin that obey Bose-Einstein statistics, which allow two or more identical particles to occupy the same quantum state simultaneously. The gauge bosons that mediate the electromagnetic, weak, and strong interactions are all spin-1 particles.

Table 1.3: Gauge bosons and their properties [4].

Boson	Charge (/e)	Mass ($\times c^2$)	Interaction
γ (photon)	0	0	Electromagnetic
$W^{\pm}$	± 1	80.419 GeV	Weak
Z^0	0	91.188 GeV	Weak
g (gluon)	0	0	Strong

The electromagnetic interaction is associated with the exchange of virtual photons between charged particles, and for this reason photons are said to *couple* to charge. The strength of the interaction is proportional to the charge on a particle and is characterised by the *fine structure constant*. In natural units ($\hbar = c = 1$) the fine structure constant, α, is

$$\alpha = \frac{e^2}{4\pi} \approx \frac{1}{137} \tag{1.1}$$

where e is known as the *coupling constant* and is equal to the electron charge magnitude in Heaviside-Lorentz units ($\epsilon_0 = \mu_0 = 1$). The electromagnetic interaction has an infinite range. The long-range nature of the force is related to the fact that the photon is massless. This can be seen by invoking the uncertainty principle

$$\Delta E \Delta t \approx \hbar. \tag{1.2}$$

An estimate of the maximum range of the force, R, is $c\Delta t$. With $\Delta E = mc^2$,

$$R \approx c\Delta t = \frac{\hbar c}{\Delta E} = \frac{\hbar}{mc}. \tag{1.3}$$

Thus the range of the force is inversely proportional to the mass of the exchange boson.

The weak force is mediated by the $W^{\pm}$ and Z^0 bosons and is felt by both quarks and leptons. They are very massive, and the resultant force is short range. The mass of the $W^{\pm}$ and Z^0 accounts for the low rates observed for weak decays. The masses of the Z^0 is almost one hundred times that of the proton. The weak and electromagnetic interactions can be regarded as two different aspects of a unified *electroweak* interaction, in the same way that electrostatic and magnetic forces are two different aspects of electromagnetism. It is theorised that at high energies the weak and electromagnetic coupling constants converge to a single value. Unification of the weak and electromagnetic forces lead to a prediction of the $W^{\pm}$ mass that can be tested. The $W^{\pm}$ mass was measured at the LEP, and is in good agreement with the predicted value. Interactions involving $W^{\pm}$ bosons are called *charged current processes* because they change by one unit the charge of the quarks or leptons they couple to. Interactions involving the Z^0 do not exhibit this behaviour and are known as *neutral current processes.*

The strong force is mediated by gluons — of which there are eight types — and is felt by quarks. Gluons couple to colour, but also carry colour. Consequently, they interact not only with the quarks but also with each other. Gluons are massless, but this does not lead to a force of infinite range. In fact, the strength of the force between quarks increases as the distance between them increases. This aspect of gluon interactions is responsible for the short-range nature of the strong force.

The origin of mass

The Standard Model does not explain the observed masses for quarks and leptons, or the large differences in mass between the quark and lepton generations. It does not explain the masses of the $W^{\pm}$ and Z^0. The particle masses are all free parameters of the theory. This situation is untenable. Naively one might ask why the Standard Model cannot be formulated entirely in terms of massless particles, and then add mass terms afterwards. However, the resulting theory is fundamentally defective.

1.2 Experimental methods

In particle physics the measured quantities are cross sections and decay rates. These two observables are the interface between experiment and theory.

Cross sections

The cross section σ is a measure of the probability of an encounter between particles that will result in the occurrence of a specified reaction. It depends only on the nature of the interaction, and can be thought of as an imaginary area through which an incident particle must pass for the interaction to occur. Cross sections are expressed in units of area; the unit used is the *barn*, defined as 10^{-24} cm^2. The total number N of scattering events for specified process is equal to the cross section for that process multiplied by the integral of the luminosity over time:

$$N = \sigma \int \mathcal{L}\, dt. \tag{1.4}$$

In a colliding-beam experiment the luminosity $\mathcal{L}$ is the number of particles in the beam per unit area per unit time. The units of luminosity are cm^{-2}s^{-1}. Luminosity is sometimes expressed in nb^{-1}, pb^{-1}, or fb^{-1}. Typically, the cross section for a process is measured by observing many interactions, counting the number of those that resulted in a particular type of event, and dividing that number by the integrated luminosity. Because they quantify the probability of a process occurring it is said that cross sections are bounded to lie below the *unitarity limit*.

Decay rates

Quantum mechanics predicts that the proper decay time of unstable particles will follow an exponential probability distribution. The total decay rate Γ is equal to the reciprocal of the mean lifetime τ. The partial decay rate Γ_i is defined to be the total rate Γ multiplied by the probability $\mathcal{B}$ for the decay to result in the final state i. This probability is known as the *branching ratio* for the final state i.

Invariant mass and other useful quantities

The *invariant mass* M of a system of n particles with energies E_i and momenta $\mathbf{p}_i$ is defined to be

$$M = \sqrt{E^2 - \mathbf{P}^2} \tag{1.5}$$

where

$$E = \sum_{i=1}^{n} E_i \quad \text{and} \quad \mathbf{P} = \sum_{i=1}^{n} \mathbf{p}_i. \tag{1.6}$$

Other useful quantities are:

$$p_T = \sqrt{{p_x}^2 + {p_y}^2} \tag{1.7}$$

$$E_T = \sqrt{{p_T}^2 + m^2} \tag{1.8}$$

$$\phi = \tan^{-1}\left(\frac{p_y}{p_x}\right) \tag{1.9}$$

$$\theta = \tan^{-1}\left(\frac{p_T}{p_z}\right) \tag{1.10}$$

$$\eta = -\ln\tan\left(\frac{\theta}{2}\right) \tag{1.11}$$

$$\Delta R = \sqrt{\Delta\eta^2 + \Delta\phi^2} \tag{1.12}$$

where p_T is the transverse momentum, E_T is the transverse energy, and m is the mass of the particle. p_x, p_y, and p_z are the x, y, and z components of momentum, respectively. ΔR expresses the separation in $\eta - \phi$ space between objects. The beam direction defines the z-axis. The positive x-axis is defined to point from the interaction point to the centre of the LHC ring. The positive y-axis points upwards, perpendicular to the plane of the LHC ring. The azimuthal angle ϕ is measured around the beam axis, and the polar angle θ is the angle from the beam axis.

1.3 Basic theoretical concepts

The Standard Model is an example of a quantum field theory. These are theories in which particles are treated as fields. One of the fundamental tenets of quantum field theory is the principle that for every reaction there is an associated *amplitude*, and that if a reaction can proceed by more than one path, the total amplitude is the sum of the amplitudes for each path. There are, in fact, an infinite number of different paths by which a particle physics interaction may proceed. The simplest of these might, for example, correspond to the exchange of a single gauge boson between fermions. The paths become progressively complex as those that involve a greater number of intermediate particles or gauge boson couplings are considered. The different paths correspond to terms in a *perturbation series.* Progressively complex paths are associated with higher-order terms in the series. These higher-order terms act as small corrections to the total amplitude, if the perturbation expansion is valid.

The cross section for a reaction is proportional to the absolute square of the total amplitude. This prescription for computing cross sections is known as *perturbation theory.* Usually the terms in perturbation theory are depicted pictorially by Feynman diagrams, which are schematic representations of particle reactions.

The parts of the Standard Model which describe electromagnetic and strong interactions are known as Quantum Electrodynamics (QED) and Quantum Chromodynamics (QCD), respectively. Before perturbation theory can be used with QED and QCD to compute cross sections, an additional mathematical technique is needed, because it is found that without it the cross sections exceed the unitarity limit; the amplitudes corresponding to higher-order terms in the perturbation series give rise to infinities. These infinities are eliminated using a mathematical trick called *renormalisation*, developed by the architects of QED. This ensures that the cross sections do not exceed the unitarity limit.

1.4 Symmetries

The concept of symmetry has a special place in particle physics. The Standard Model explains particle physics phenomena in terms of symmetries and the breaking of symmetries. The form of the theory is determined by the symmetries respected by nature.

There is a fundamental connection between symmetries and conservation laws. In general, the existence of a symmetry implies the existence of an associated conservation law. If a physical system is invariant with respect to a transformation U it is said that U is a symmetry of the system. A corollary is that U is a symmetry if it leaves the Hamiltonian H of the system invariant, or equivalently, if U commutes with the Hamiltonian.

Local gauge symmetry plays a crucial role in particle physics. Its existence in a theory implies that globally-conserved physical quantities, such as charge or colour, are conserved in local regions of space also. In particle physics, invariance of the Lagrangian density under gauge transformations is treated as a fundamental requirement of quantum field theories. This is called the *gauge principle*. Quantum field theories based on this principle are called *gauge theories*. QED and QCD are both gauge theories. The gauge principle forces the introduction of vector fields to the QED and QCD Lagrangian densities. The quanta of these fields are the gauge bosons. Moreover, demanding that the QED and QCD Lagrangian densities are locally gauge invariant requires that the photon and gluon are massless. It turns out that all renormalisable quantum field theories must be gauge theories involving the exchange of gauge bosons [7].

Adding mass terms to the Lagrangian densities of gauge theories destroys the gauge symmetry. This is the reason for requiring that the photon and gluon are massless. However, the $W^{\pm}$ and Z^0 bosons that mediate the weak interaction are massive. This is a serious problem, because the addition of mass terms to the Lagrangian density breaks the gauge symmetry, and the resulting theory is unrenormalisable. Infinities appear that cannot be eliminated. No predictions are possible, and the theory is meaningless. Therefore there must be some mechanism that allows for massive particles without breaking the gauge symmetry. This is the *Higgs mechanism* [8].

1.5 The Higgs mechanism

In the Higgs mechanism, the particle masses are not introduced directly into the theory. Instead, the Lagrangian density includes a term corresponding to the Higgs field. It is the Higgs field that is responsible for imparting mass to the particles. This field is unusual in that its state of lowest energy is non-zero. Recall that in quantum field theory particles are treated as fields. The state of lowest energy for the usual Standard Model fields corresponds to there being no particles present. The resulting theory is renormalisable because the Higgs mechanism respects the gauge symmetry of the Lagrangian density.

In the same way that photons are quanta of the electromagnetic field, Higgs bosons are quanta of the Higgs field. The simplest version of the Higgs mechanism predicts the existence of one electrically-neutral scalar (that is, spin-0) Standard Model Higgs boson, denoted H.

1.6 Higgs boson searches

The Higgs boson couples to mass. The strength of the coupling is proportional to the mass of the particle with which the Higgs boson interacts. This implies that the Higgs boson will decay with greatest probability into a particle-antiparticle pair with the highest mass that is kinematically possible, and that there are no direct couplings to photons and gluons. The branching ratio of the Higgs boson into various final states as a function of the Higgs mass is shown in figure 1.1 [9].

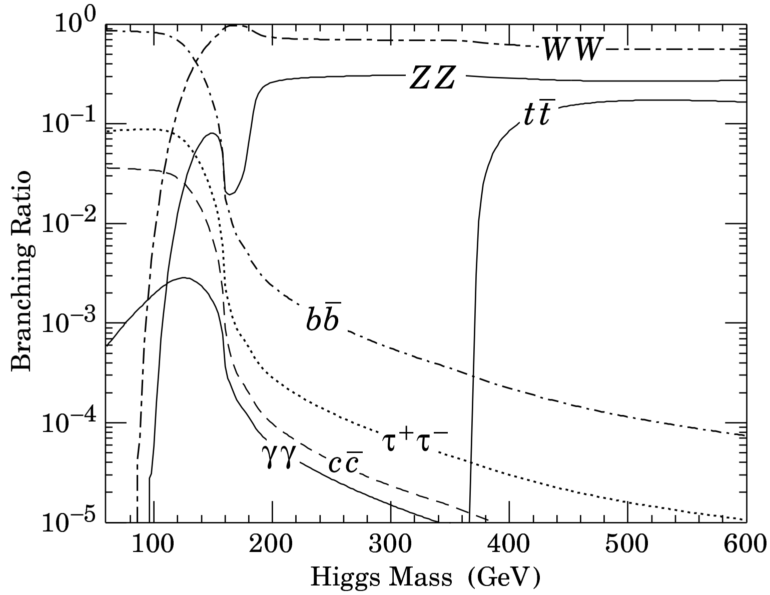

Figure 1.1: Branching ratios for the main decay modes of the Higgs boson [9].

The mass of the Higgs boson itself is not predicted by theory, but it believed to be less than 1 TeV/c^2, because the Higgs boson is self-interacting and the couplings are required to be sufficiently weak such that perturbation theory is applicable [10]. Experimental searches at the LEP have excluded a large range of Higgs boson masses. The existence of a Higgs boson with a mass less than 100 GeV/c^2 has been ruled out.

Tantalising signs of a Higgs boson with a mass of 115 GeV/c^2 were found at the LEP during the summer of 2000 [11]. The LEP was scheduled to close at the end of September that year, but a five-week extension of running was granted by

CERN[1] in an attempt to confirm or rule out the signal. Unfortunately, the new data was not sufficiently conclusive to announce a discovery. The LEP finally closed on 2 November 2000 to make way for construction of the Large Hadron Collider (LHC).

If the mass of the Higgs boson, m_H, is indeed 115 GeV/c^2, then it will decay with greatest probability into a $b\bar{b}$ pair, as shown in figure 1.1 [9]. A peak at m_H in the distribution of the invariant mass of all possible $b\bar{b}$ pairs would indicate the presence of the Higgs boson.

[1] CERN: Conseil Européen pour la Recherche Nucléaire

Chapter 2

Detector simulation

2.1 ATLAS and the LHC

The Large Hadron Collider (LHC) is a next-generation collider that will be installed in the existing LEP tunnel at CERN. The LHC is primarily a proton-proton collider, but can also be used as a heavy-ion (Pb-Pb) collider. The LHC will be fed by existing particle sources and pre-accelerators. In proton-proton collider mode the beam energy will be 7 TeV. The resultant total centre-of-mass energy will be 14 TeV. The beam lifetime is 10 hours. The initial luminosity will be 10^{32} $\mathrm{cm}^{-2}\,\mathrm{s}^{-1}$.

The ATLAS detector

The ATLAS (A Toroidal LHC ApparatuS) detector will study proton-proton interactions and is due to begin operation in 2006. ATLAS will be capable of exploring a new energy regime, and will search for Higgs bosons, supersymmetric particles, quark substructure, and physics beyond the Standard Model.

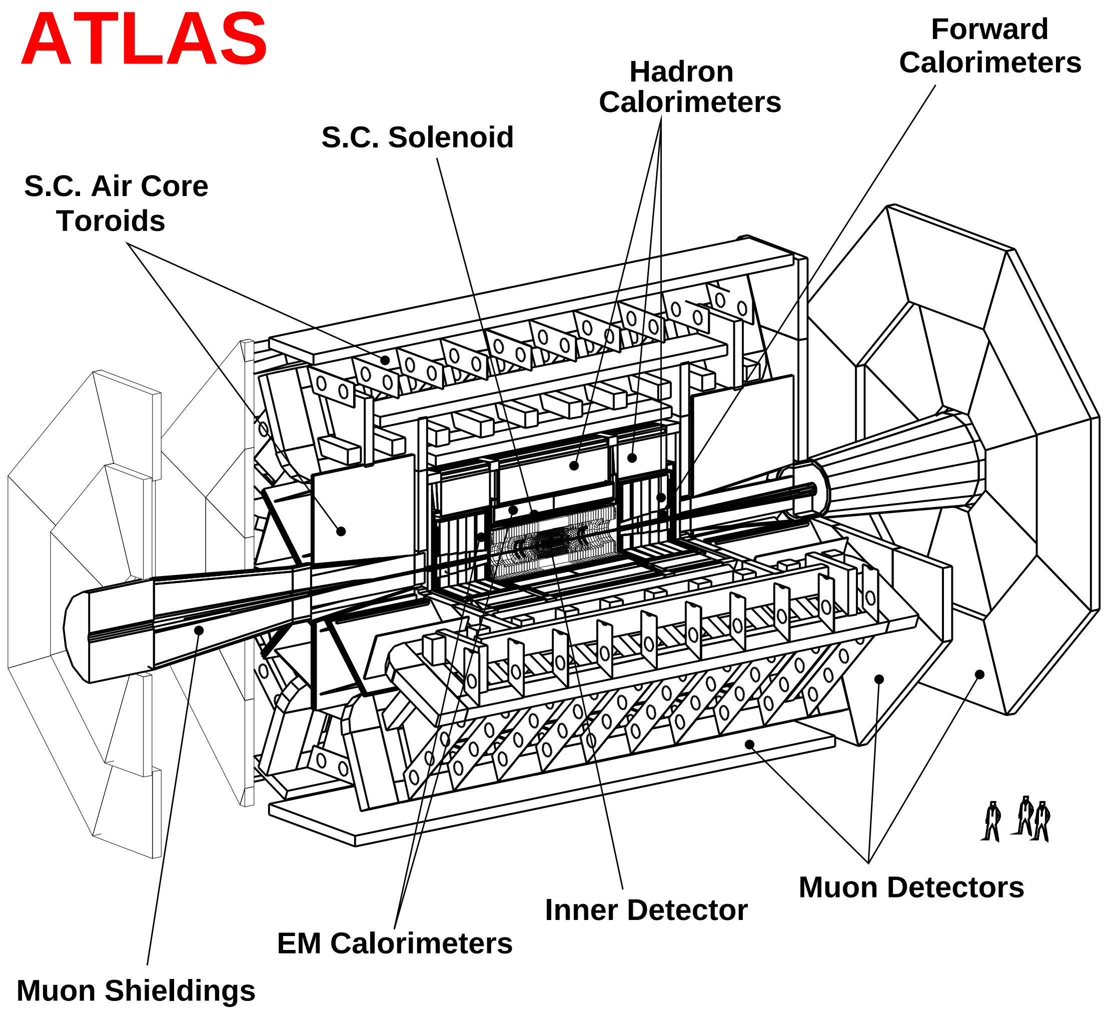

Figure 2.1: The ATLAS detector.

B-tagging

When a particle decays to a q$\overline{\text{q}}$ pair, each quark produces a spray of hadrons known as a *jet*. The quarks are said to *hadronise*. In order to observe decays of Higgs bosons into $b\bar{b}$ pairs, the ATLAS detector needs to be able to identify the two jets that resulted from the $b\bar{b}$ pair. Each *b-jet* will contain a hadron with a b quark. These hadrons will travel a few millimeters within the detector before decaying. The tracks of the decay products will not point back to the interaction point. ATLAS uses this information to identify b-jets. This is known as *b-tagging*. At low luminosity the b-tagging efficiency of the ATLAS detector is about 60% [10].

2.2 The WH channel

Figure 1.1 shows that the branching ratio for $H \rightarrow b\bar{b}$ is is 90% at $m_H \approx$ 115 GeV/c^2 [10]. Associated production with a $W^{\pm}$, Z^0, or $t\bar{t}$ are the only possible processes available for observing a signal from $H \rightarrow b\bar{b}$ decays. Direct production $gg \rightarrow H$ with $H \rightarrow b\bar{b}$ cannot be efficiently triggered or cleanly extracted as a signal above the huge QCD jet background. The leptonic decay of the $W^{\pm}$ provides an isolated high-p_T lepton for triggering. The Higgs boson signal is seen as a resonant peak in the invariant $b\bar{b}$ mass distribution. The high-p_T lepton is useful for rejecting the large QCD jet background.

The ATLAS TDR [10] examined the feasibility of discovering the Higgs boson using the channel $WH(H \rightarrow b\bar{b})$. The study in the TDR was based on work by the same authors published earlier [12], which was, in turn, based on an earlier feasibility study for discovering the Higgs boson using $H \rightarrow b\bar{b}$ at LEP II, the Tevatron, and the LHC [14].

The WZ process constitutes a major resonant background for the WH signal. It is expected that the distribution of invariant $b\bar{b}$ mass has two resonant peaks; one peaked at the Z^0 mass, and another, much smaller, peaked at the Higgs boson mass. The Higgs resonance comes from the $(q^2 - {m_H}^2)^{-1}$ factor in the amplitude, where $q^2 = q^\mu q_\mu$ is the Higgs boson four-momentum squared and m_H is the Higgs boson mass. Hopefully the Higgs resonance is detectable. Excellent b-tagging will be required.

At high luminosity (10^{34} cm^{-2} s^{-1}) $WH(H \to b\bar{b})$ is not so promising a channel for discovering the Higgs boson. This is because it is extremely difficult to apply tight jet veto cuts, and the resolution of the invariant $b\bar{b}$ mass is degraded.

This channel complements the search for the Higgs boson using the channel $H \to \gamma\gamma$, which is the cleanest channel, but more rare, as shown in figure 1.1. The $WH(H \to b\bar{b})$ channel is also worth studying because it could provide valuable insights into the coupling of the Higgs boson to $W^\pm$ bosons and b quarks.

The virtual $W^\pm$ radiates a Higgs boson to become more *on-shell* (that is, less virtual). The process can be called *Higgsstrahlung*, and is illustrated in figure 2.2.

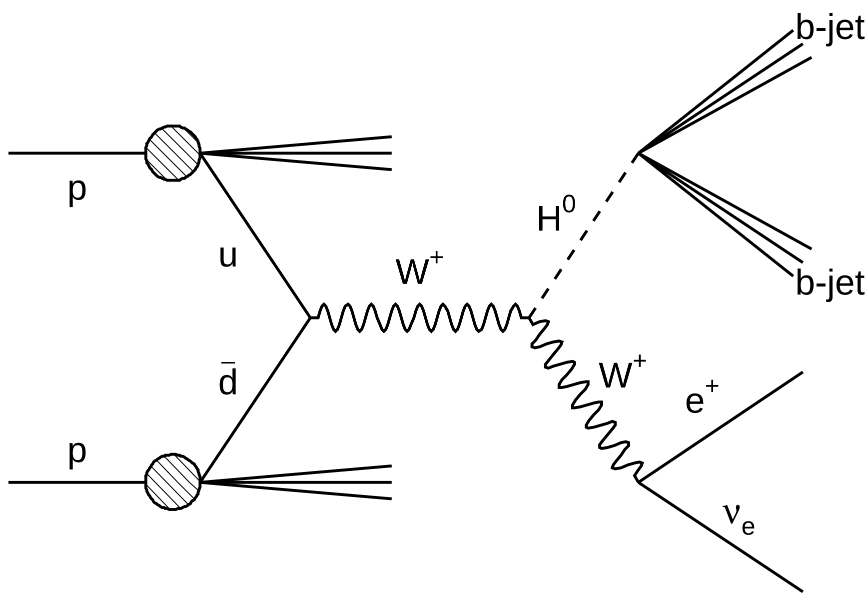

Figure 2.2: A Feynman diagram for the WH (signal) process.

Figure 2.3 shows what the signal process looks like in the ATLAS detector. The two forward-backward peaked jets are the remnants of the proton-proton collision. These mask the tiny contribution to the missing momentum that is attributed to the neutrino resulting from the leptonic decay of the $W^{\pm}$.

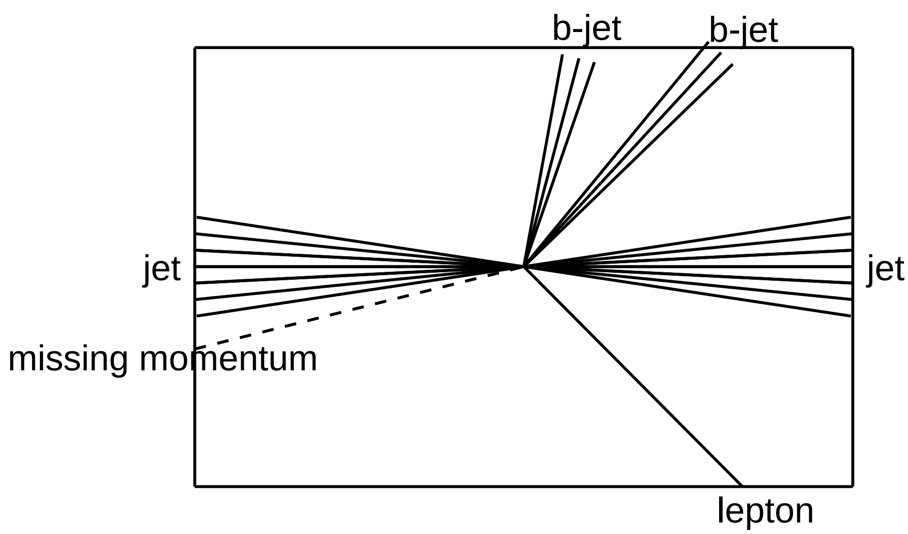

Figure 2.3: Signal event as seen by ATLAS.

2.3 Backgrounds

The backgrounds to the WH signal are everything that can happen in a proton-proton collision. Obviously it would take too long to compute every possible background process. However, most of the pp cross section does not look like the signal process. It is possible to limit the backgrounds to be considered to a small subset of processes that look like the signal process. The important background processes are:

- $WZ \rightarrow l\nu b\bar{b}$
- $q\bar{q} \rightarrow W^* \rightarrow \bar{t}b \rightarrow Wb\bar{b}$
- $t\bar{t} \rightarrow WWb\bar{b}$

- $gq \to t\bar{b}q \to l\nu b\bar{b} + q$
- $q\bar{q} \to Wg \to Wb\bar{b}$
- Wjj

Figure 2.4 shows the WZ background process. The final state is indistinguishable from that of the signal process. Such backgrounds are said to be *irreducible.* The mass cut should eliminate the bulk of this background. Some WZ events will survive this cut because the invariant $b\bar{b}$ mass distribution has a long tail that protrudes into the mass cut window.

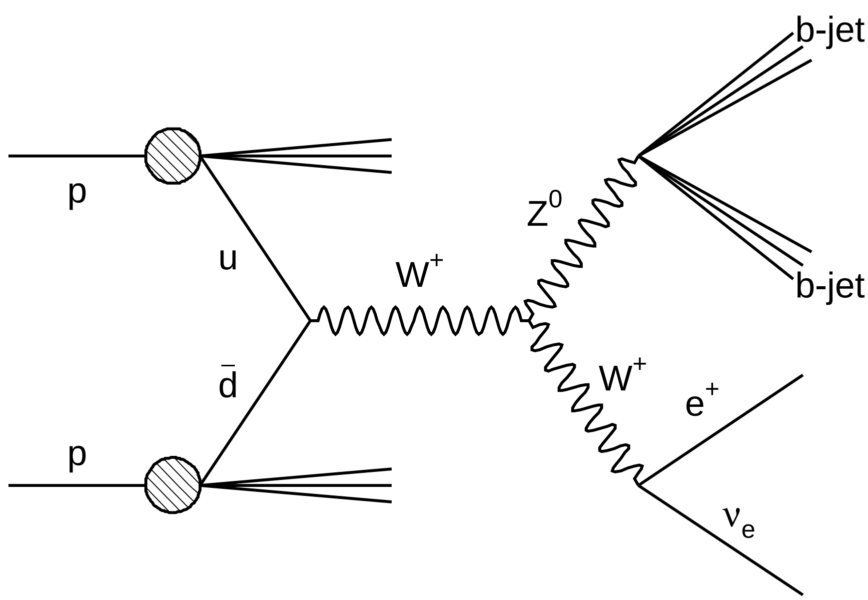

Figure 2.4: A Feynman diagram for the WZ background process.

Another irreducible background is $q\bar{q} \to Wg \to Wb\bar{b}$, shown in figure 2.5. The process $t\bar{t} \to WWb\bar{b}$ (see figure 2.6) constitutes a *reducible* background. It arises when one of the $W^{\pm}$ bosons is missed. This is the biggest background to the WH signal for $m_H > 80$ GeV/c^2 [14]. Vetoing any additional high-p_T leptons or jets in the final state should reduce this background.

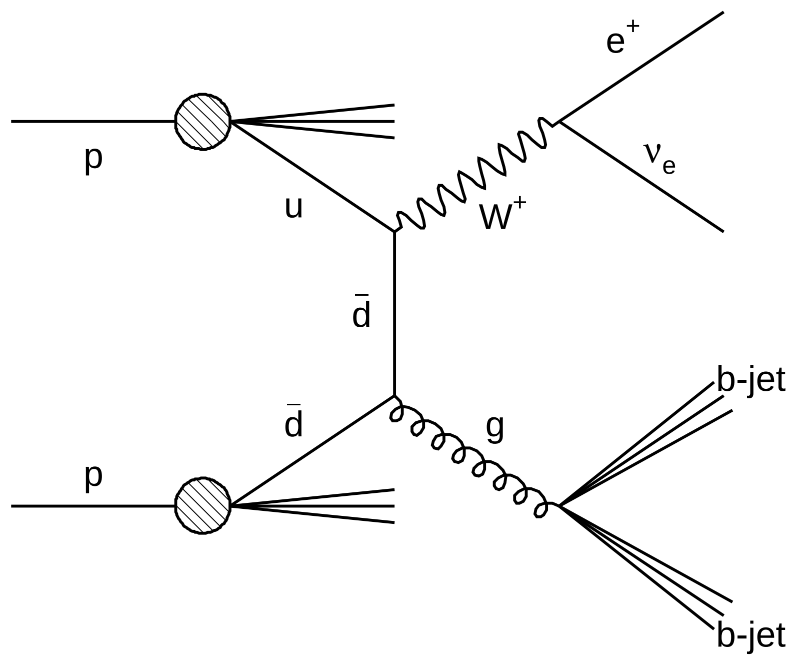

Figure 2.5: A Feynman diagram for the $Wb\bar{b}$ background process.

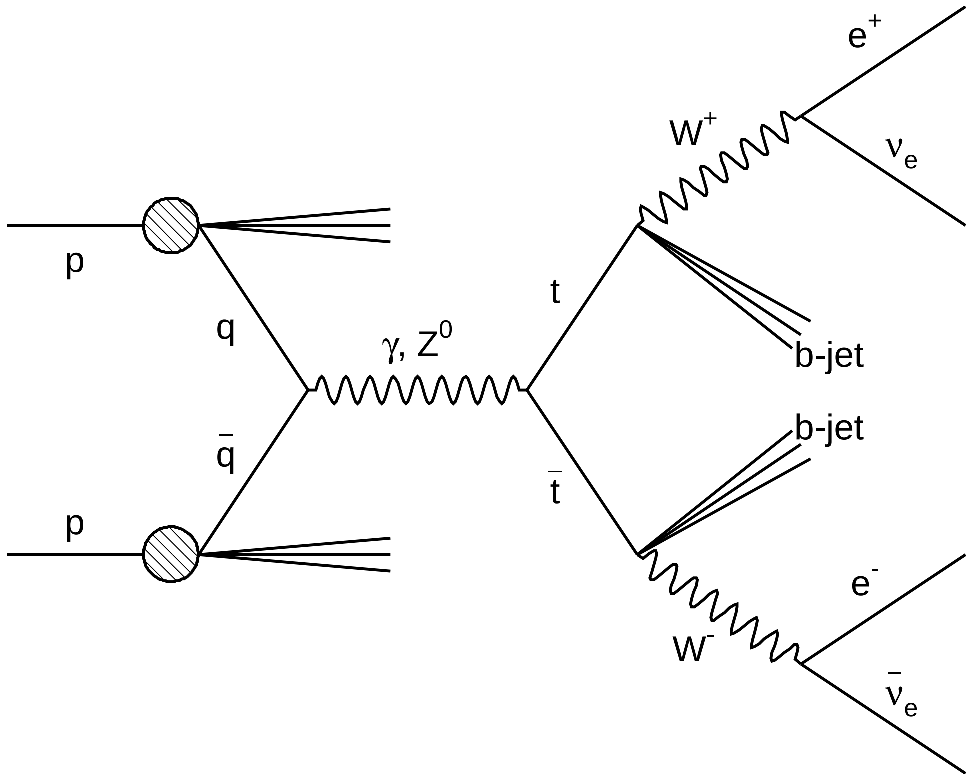

Figure 2.6: A Feynman diagram for the $t\bar{t} \rightarrow WWb\bar{b}$ background process.

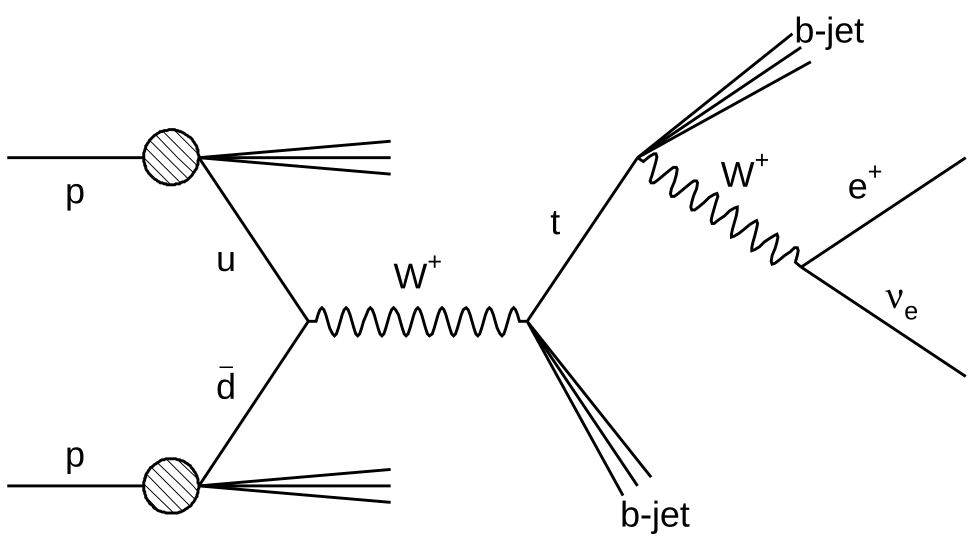

Figure 2.7: A Feynman diagram for the $W^* \rightarrow \bar{t}b \rightarrow Wb\bar{b}$ background process.

Cuts are applied to reduce these backgrounds. By applying different cuts it is hoped that a bigger fraction of the background events are thrown away than the signal events, therefore enhancing the signal.

The selection criteria for the WH channel are:

- One isolated trigger electron with $p_T > 20$ GeV/c within $|\eta| < 2.5$, or one isolated trigger muon with $p_T > 6$ GeV/c within $|\eta| < 2.5$,
- Two tagged b-jets with $p_T > 15$ GeV/c within $|\eta| < 2.5$,
- Lepton veto: no additional lepton with $p_T > 6$ GeV/c within $|\eta| < 2.5$,
- Jet veto: no additional jet with $p_T > 15$ GeV/c within $|\eta| < 5$,
- Mass cut: events are kept if the invariant mass of the two tagged b-jets is within a mass window of ± 22 GeV/c (that is, $\pm 2\ \sigma_m$) around the nominal Higgs boson mass.

These selection criteria can be achieved at low luminosity (10^{32} cm^{-2} s^{-1}) [12]. *Isolated* means $\Delta R = \sqrt{\Delta\eta^2 + \Delta\phi^2} > 0.7$ from any other particle or jet. PYTHIA 6.1 [16] was used to generate both the signal and all the background processes. Atlfast was used to simulate the effect of the detector on these events.

2.4 Event generation with Pythia

PYTHIAčiteSjostrand:1994yb is an event generator; it uses knowledge of real particle physics phenomena to generate events. PYTHIA is a Monte Carlo simulation of particle physics processes. Atlfast takes the output of PYTHIA and simulates the effect of the detector. Atlfast simulates how particles travel in the detector, produce showers in the calorimeters, or sneak out through cracks. To simulate just a single event using a full simulation of the detector, using detailed knowledge of the detector and the physics, takes hours of days. This is clearly too long if the user simply wants to test the feasibility of getting an observable signal for a new particle using a particular channel. Fast simulations do not use such detailed information about the detector and run much faster, enabling the user to reject channels that prove to be unsuitable, and therefore need not be simulated in full.

2.5 Atlfast-Athena

Atlfast-Athena was written in C++ and was run under the operating system Red Hat Linux 6.0. Athena is the name of the control framework developed for ATLAS. Athena evolved from an earlier framework called Gaudi, and inherits much of its functionality. A framework is a skeleton of an application into which developers plug in their code. An example class, called *ExampleAnalysis*, was provided with the source code and is designed to show new users how to access and use Atlfast objects. This class books memory for a one-dimensional histogram of isolated electron $\mathrm{p_T}$, fills the histogram by iterating over all the isolated electrons in each event and binning the data, and sends information about each electron to standard output.

Atlfast-Athena makes extensive use of classes defined within the Standard Template Library (STL) and Athena/Gaudi library. The STL provides basic class templates for handling objects such as strings, vectors, algorithms, and containers. The Athena/Gaudi library contains templates for Athena algorithms, message streams, collections, and histogram services. An Athena algorithm is a specialised class, scheduled and controlled by the framework, for processing data. Athena algorithms inherit from the algorithm base class provided by the STL. ExampleAnalysis is an Athena algorithm class. Message streams are classes that provide a way of passing information to standard output, and allow the user to define the verbosity of the output at runtime.

Collections are specialised container classes for storing data objects. For example, *JetCollection* contains data objects that represent jets. Data objects that represent physical entities, like particles and jets, have methods that when called return information like the position in $\eta - \phi$ space of the object, its p_T, or its four-momentum. Data objects of this type are usually accessed via specialised pointers.

Histogramming services are provided by HBOOK, which is a FORTRAN package from CERN for statistical analysis and fitting. HBOOK contains subroutines that can be called from Atlfast for creating and manipulating histograms and tables of data called n-tuples. An interface is provided by CERN so that the FORTRAN HBOOK subroutines may be called from C++ code. HBOOK writes histogram files that can be read, and the data within manipulated and graphically presented, by analysis tools such as PAW (Physics Analysis Workstation) and ROOT. The former of these tools is also provided by CERN, and is popular among particle physicists for analysing and plotting data.

Athena algorithms have properties that can be set at runtime via the *jobOptions* file. Only Athena algorithms have properties that can be set this way. The jobOptions file informs Athena to load the relevant libraries needed by Atlfast, sets the configuration options, and allows the user to over-write the hard-coded default values of the analysis parameters with their own values.

This study involved using the new C++ version of Atlfast to replicate the results published in the ATLAS TDR.

Chapter 3

Analysis

The ExampleAnalysis class that is provided with the source code fills a histogram with the p_T of a handful of isolated electrons. It is easy to alter the jobOptions file so that more events are generated. The different switch settings are listed and explained in detail in the PYTHIA manual [15]. This study used PYTHIA version 6.1. There are some slight differences in the naming of some switches between the earlier version (5.7) and version 6.1. An interface, called *PythiaModule*, exists between PYTHIA and Athena. The interface allows jobOption switch settings to be passed from Athena into PYTHIA.

After examining the source code for the different classes in detail, the other variables that may be binned in a histogram (energy, pseudorapidity η, azimuthal angle ϕ, E_T, etc.), were determined. The code also indicates how to calculate variables like the invariant mass of a pair or a collection of particles/jets.

The event data generated by Atlfast-Athena is stored in memory in what is known as the *Transient Event Store* (TES). Isolated electrons are located in the TES at *"event/AtlfastIsolatedElectrons"*. The location of other data objects is quite transparent. However, simply replacing the address for isolated electrons in the TES with the address for jets in the TES does not work. Particles and jets are two differently coded object types. Particles are of type *ReconstructedParticle*, jets are of type *Jet*. Their collection types are ReconstructedParticleCollection and JetCollection, respectively. They are accessed via *smart data pointers* that are provided by Athena. An *iterator* can be defined for these container types, which allows the user to reference a particular particle within a particle collection, or a jet within a jet collection. To generate histograms of, say, jets, both the correct location within the TES for jets, and the container type JetCollection, must be given. Both ReconstructedParticles and Jets have methods that return the four-momentum of the object. This enables the invariant mass of a set of objects to be calculated.

The ExampleAnalysis code was broken up into small classes that each serve a particular function, and further classes were written to assist in the analysis. The class *ObjectDumper* was written for examining each collection type and directing information via message streams about electron, muon, and jet multiplicities and p_T to standard output. Multiplicity histograms are the of all histograms to fill because the size of a collection can be returned using their *size* method. The class *MultiplicityHistogram* performs this function. Histograms that require the use of an iterator to examine the contents of each collection are filled by *HistogramFiller*. The class *HiggsCandidate* is responsible for deciding which events to keep, by applying the selection criteria to the event.

Job options for Atlfast are set via the file *StandardAtlfastOptions*. For this study, two switches in particular have a detrimental effect on the results if set incorrectly: smearing must be turned *on* for all particle and jet makers, and luminosity must be set to *low*.

Note that in this study the efficiency of the b-tagging was assumed to be 60%.

Pythia switch settings

The following PYTHIA switch settings were common to *all* processes studied:

- Proton parton distribution set CTEQ2L. This is the same structure function parameterisation that was used for the Higgs boson studies in the ATLAS TDR. The parton distribution function parameterises the probability to "pull" a parton from a proton with a particular momentum.

- Allow the top to decay. It is known that the top quark cannot form hadrons.
- The top quark mass is set equal to 175.0 GeV/c^2.
- The choice of longitudinal fragmentation function is the *hybrid scheme* [15].
- SLAC parameterisation of fragmentation function chosen [15].

  (PARJ(54) = -0.07 and PARJ(55) = -0.006 [12].)

The switch settings required to generate each process are listed below.

- For $WH(H \to b\bar{b})$:

  Process 26: $f_i\overline{f_j} \to W^{\pm}H^0$

  Desired subprocesses must be switched on.

  All decays of $W^{\pm}$ except $W \to e + \nu_e$ and $W \to \mu + \nu_\mu$ turned off.

  All decays of Higgs boson except $H \to b\bar{b}$ turned off.

- $WZ \to l\nu b\bar{b}$:

  Process 23: $f_i\overline{f_j} \to Z^0W^{\pm}$.

  Desired subprocesses must be switched on.

  All decays of $W^{\pm}$ except $W \to e + \nu_e$ and $W \to \mu + \nu_\mu$ turned off.

  All decays of Z^0 except $H \to b\bar{b}$ turned off.

- $q\bar{q} \to W^* \to \bar{t}b \to Wb\bar{b}$:

  Process 2: $f_i\overline{f_j} \to W^{\pm}$.

  Desired subprocesses must be switched on.

  Kinematic cut: CKIN(1) = 184.5 $(m_t + m_b)$.

  Kinematic cut: CKIN(2) = -1.0.

- $t\bar{t} \to WWb\bar{b}$:

  Process 6: $t\bar{t}$ production with massive matrix elements.

  Allow top to contribute to cross sections.

- $gq \to t\bar{b}q \to l\nu b\bar{b} + q$:

  Process 83: $q_i f_j \to Q_k f_l$.

  Desired subprocesses must be switched on.

3.1 Results

The signal process $WH(H \to b\bar{b})$ was successfully generated. As shown in table 3.1, the expected number of signal events for an integrated luminosity of 30 fb^{-1}, which is expected to be achieved at ATLAS after three years of initial operation at low luminosity (10^{32} cm^{-2} s^{-1}), agrees with the expected number of signal events for the same integrated luminosity published earlier in the ATLAS TDR [10]. Table 3.1 shows the results for the same analysis performed with a mass of 115 GeV/c^2 assumed for the Higgs boson. A comparison of total cross sections cannot be made because the ATLAS TDR does not contain this information for an assumed Higgs boson mass of 120 GeV/c^2. As shown in figure 3.1, the distribution of the invariant mass of tagged b-jets is peaked at the Higgs boson mass, as expected.

A technical problem prevented the generation of the full 200000 signal events. Only 84251 WH events were generated. The source of the problem was found to be within HBOOK, and is common when writing large files. Unfortunately, a solution to this problem was not found in time to repeat the generation of signal events in order to accumulate more data.

The following background processes were generated successfully:

- $WZ \to l\nu b\bar{b}$
- $q\bar{q} \to W^* \to \bar{t}b \to Wb\bar{b}$
- $t\bar{t} \to WWb\bar{b}$
- $gq \to t\bar{b}q \to l\nu b\bar{b} + q$

The expected number of background events are broadly in agreement with those published in the ATLAS TDR, but there are differences that still need to be understood. The results for the WZ background agree most closely with the backgrounds studied in the ATLAS TDR. This is to be expected, because it is the easiest background to generate with Pythia once the switch settings for the signal process are known.

The fact that the signal and WZ processes agree well with the ATLAS TDR results is evidence that corroborates the belief that the source of the differences is in the event generation or in the detector simulation. This analysis has been performed using Pythia 6.1. The study described in the ATLAS TDR is based on earlier work by the same authors [12], in which the event generators used were Pythia 5.7, HERWIG 5.6, and LDW. It is possible that Pythia 5.7 and Pythia 6.1 behave differently for some processes.

Table 3.1: Results of analysis for $m_H = 120$ GeV/c^2, 200000 events.

Process	Efficiency (%)	σ_{total} (pb)	Expected number of events
WH	4.129[1]	0.208	258
WZ	0.562	0.921	155
$t\bar{t}$	0.023	364.7	2516
W^*	0.017	96.92	494
gq	0.001	2.996	0

Table 3.2: ATLAS TDR results for $m_H = 120$ GeV/c^2 [10].

Process	Efficiency (%)	σ_{total} (pb)	Expected number of events
WH	?	?	250
WZ	0.853	0.86	220
$t\bar{t}$	0.050	247	3700
W^*	} 0.053[2]	1.4	} 740[2]
gq		45	

[1] A problem with HBOOK prevented generation of 200000 events. Only 84251 WH events were generated.

[2] Combined data for W^* and gq processes. Separate values for these two processes do not appear in the ATLAS TDR.

The ATLAS TDR list expected numbers of events for three different Higgs boson masses; 80, 100, and 120 GeV/c^2. The LEP experiments have excluded the possibility of a Higgs boson with a mass less than 100 GeV/c^2. The bulk of this study was performed assuming that the Higgs mass was 120 GeV/c^2, so that the results could be compared easily with those in the ATLAS TDR. The LEP experiments hint that the Higgs boson mass is about 115 GeV/c^2. The analysis was repeated with a smaller number of events for this mass.

Table 3.3: Results of analysis for $m_H = 115$ GeV/c^2, 20000 events.

Process	Efficiency (%)	σ_{total} (pb)	Expected number of events
WH	4.325	0.254	330
WZ	1.185	0.918	326
$t\bar{t}$	0.035	365.0	3833
W^*	0.015	96.98	436
gq	0.005	3.000	5

The results of tables 3.1 and 3.2 are summarised in table 3.4, which shows the significance of the signal. Naively one might conclude from these results that a discovery at 5σ might be squeezed from ATLAS. However, the ATLAS TDR list two major backgrounds that could not be replicated for this study that could lower the significance of the signal. These backgrounds are:

- $q\bar{q} \rightarrow Wg \rightarrow Wb\bar{b}$
- Wjj

It is not known at this time how to reliably generate these events.

Table 3.4: Significance of signal, for $m_H = 115$ and 120 GeV/c^2.

Process	Expected number of events		
	Analysis results		ATLAS TDR
	115	120	120
WH	330	258	250
WZ	326	155	220
$t\bar{t}$	3833	2516	3700
W^*	436	494	} 740
gq	5	0	
Total background	4600	3165	4660
Signal/Background (%)	7.17	8.15	5.37
Signal/$\sqrt{\text{Background}}$	4.87	4.59	3.66

The invariant $b\bar{b}$ mass distribution is shown in figure 3.1 for the signal process. The mass cut has not been applied, so that the reader may see the whole distribution. The mass cut has the effect of truncating the distribution such that no bins are filled outside ± 22 GeV/c^2 of the nominal Higgs mass (120 GeV/c^2).

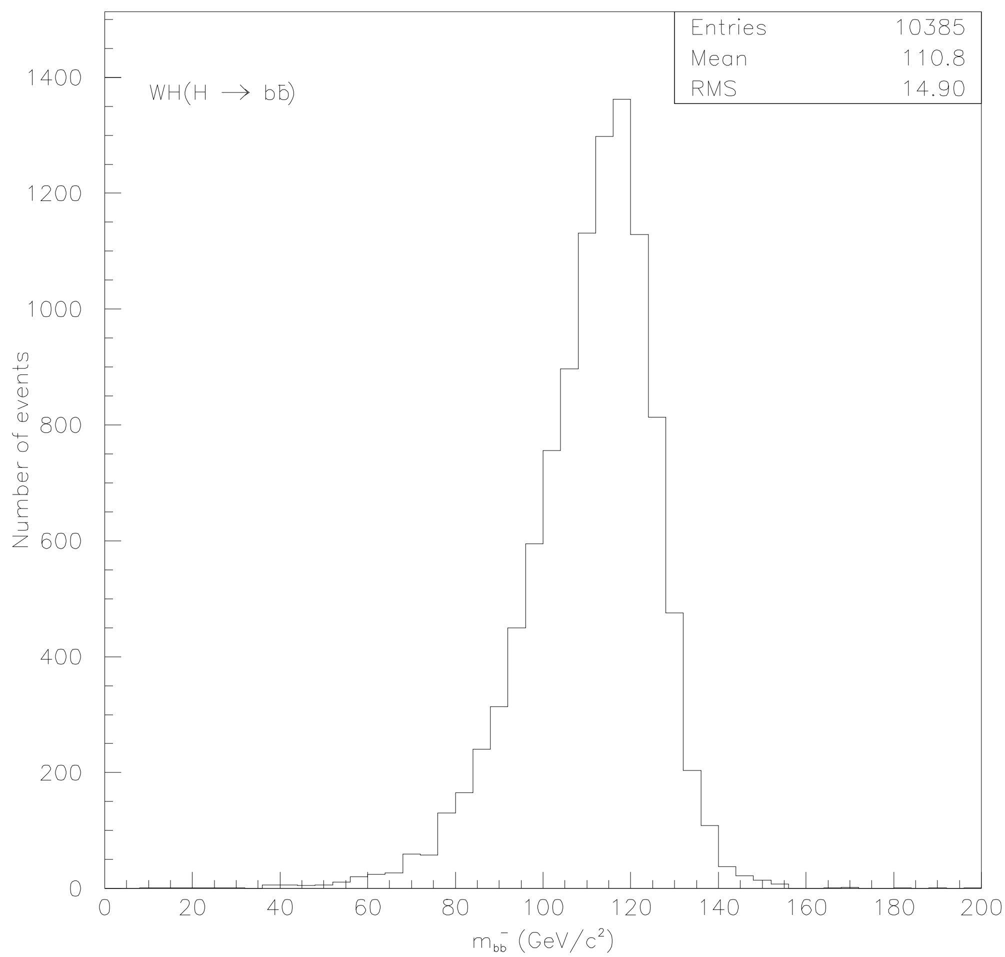

Figure 3.1: Distribution of invariant mass of tagged b-jets for signal.

Figure 3.2 shows the invariant $b\bar{b}$ mass distribution for the studied backgrounds. The distribution for the WZ process has a large resonance peak at the mass of the Z^0, as expected. The distributions for $t\bar{t}$ and W^* have a wide spread of masses. It is difficult to discern any real feature with such a small number of events. Indeed, the final background ($t\bar{b}q$) has only one event. Note that the mass cut has not been applied when producing these histograms, for the same reason that the mass cut was not applied to the same distribution for the signal events shown in figure 3.1.

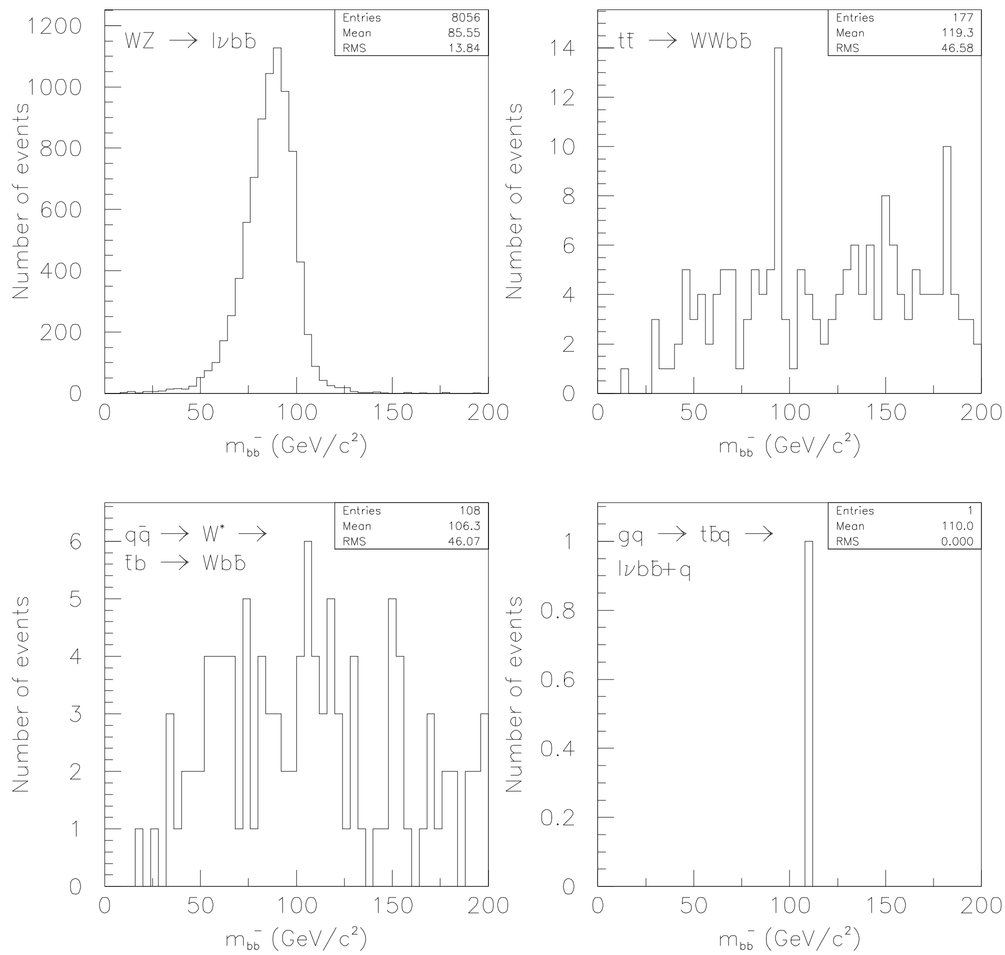

Figure 3.2: Distribution of invariant mass of tagged b-jets for backgrounds.

An interesting feature appeared when the particle identification number was binned in a histogram. All particles have a unique ID number. The antiparticles have the same number, but negative. There appear to be a statistically significant difference in the number of particle and antiparticles detected. It is not known why this is so. Note that no negative values are observed for jets. This is because the detector is not able to distinguish a jet that resulted from a b from one that resulted from a $\bar{b}$.

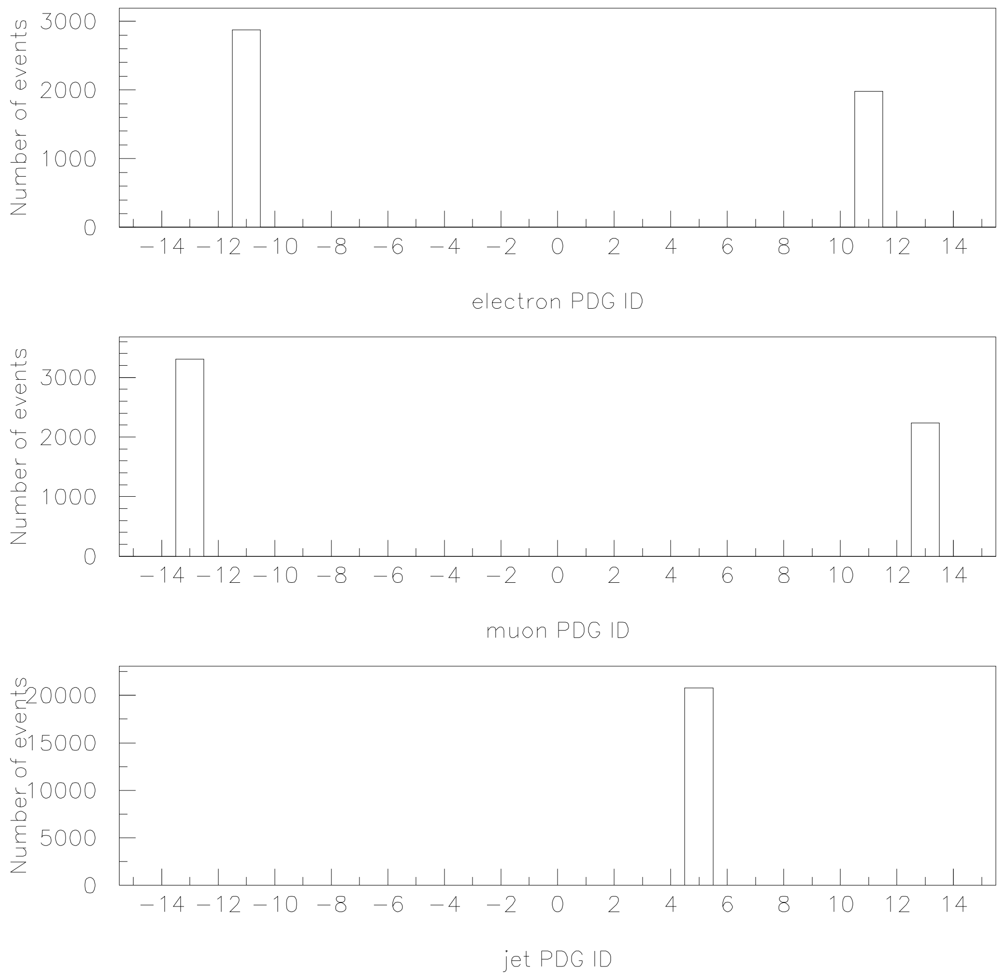

Figure 3.3: Particle and jet PDG ID numbers in signal after cuts.

It might be interesting to look at the invariant mass of the lepton and missing momentum for each event. A peak at the mass of the $W^{\pm}$ might be expected. Unfortunately, this isn't possible. The bottom right panel of figure 3.4 shows that the distribution of missing momentum pseudorapidity is very forward-backward peaked. This is due to the remnants of the proton-proton collision disappearing down the beampipe. These remnant jets form the bulk of the missing momentum.

Figure 3.5 shows the separation in $\eta - \phi$ space in the signal of b-jets, leptons and jets, leptons and b-jets, and leptons and missing momentum. The distribu-

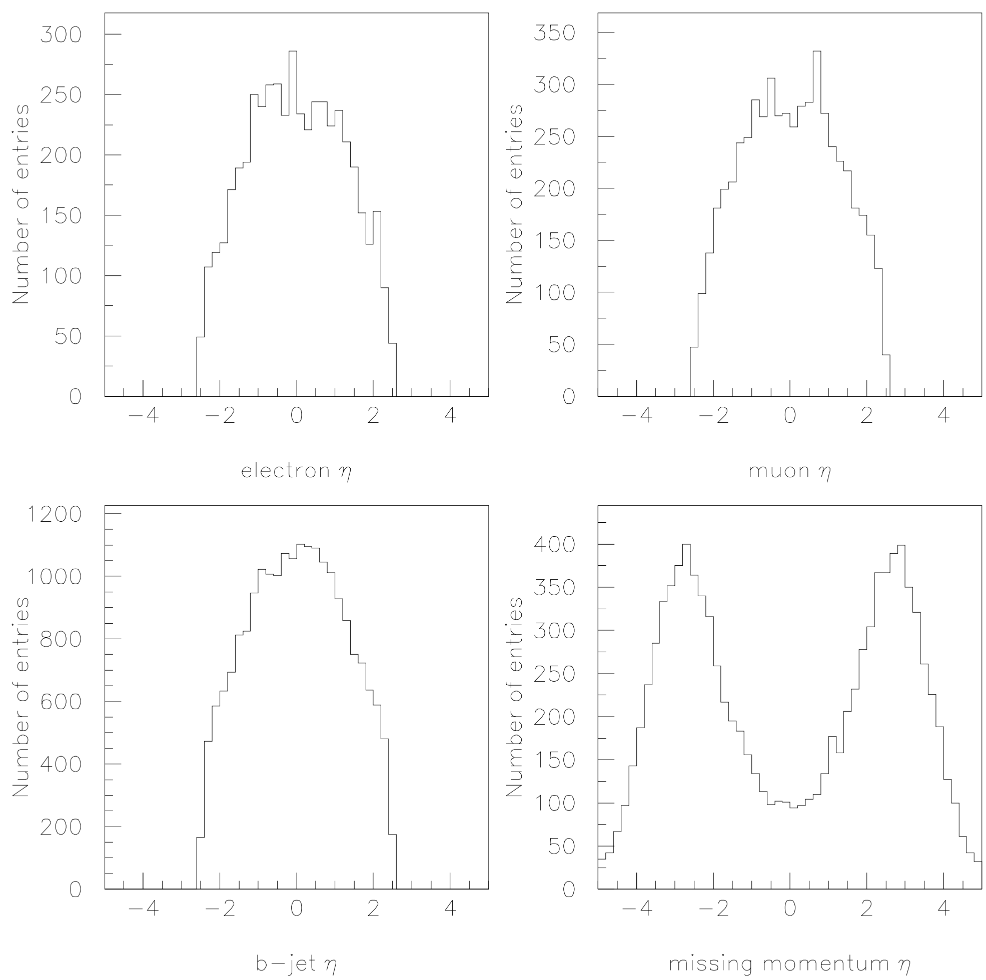

Figure 3.4: Distribution of pseudorapidity η in signal after cuts.

tion of b-jet pair separation indicates that the Higgs boson is not at rest when it decays. This is corroborated by figure 3.6, which shows b-jet pseudorapidity versus b-jet multiplicity *before* cuts. In events where only one b-jet is observed, the distribution of b-jet pseudorapidity is very forward-backward peaked. This can be explained if the separation in $\eta - \phi$ space between the two b-jets is small, and one b-jet disappears down the beampipe and is not detected.

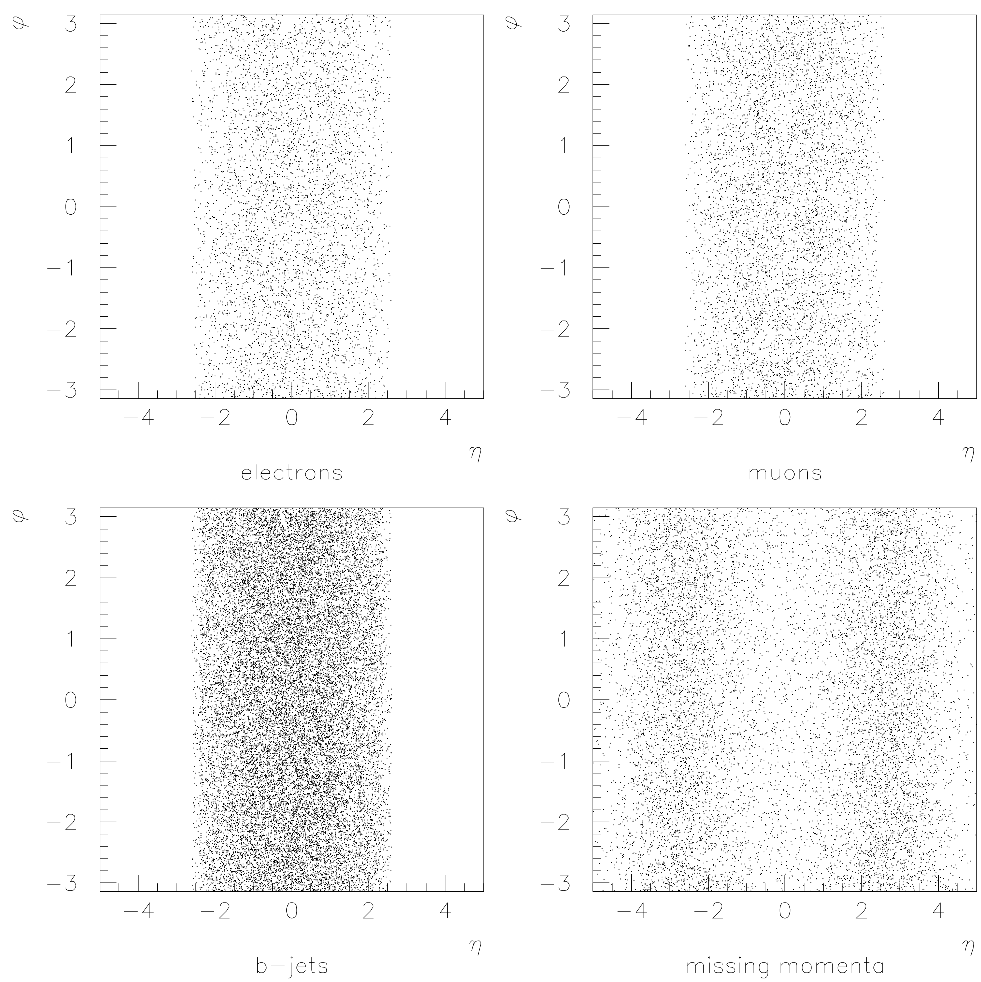

Figure 3.5: Separation of objects in signal after cuts.

In figure 3.7 it is noticed that the p_T for the WZ background process falls-off faster than that for the signal process.

In figure 3.8 is is noticed that the distributions of lepton b-jet separation in

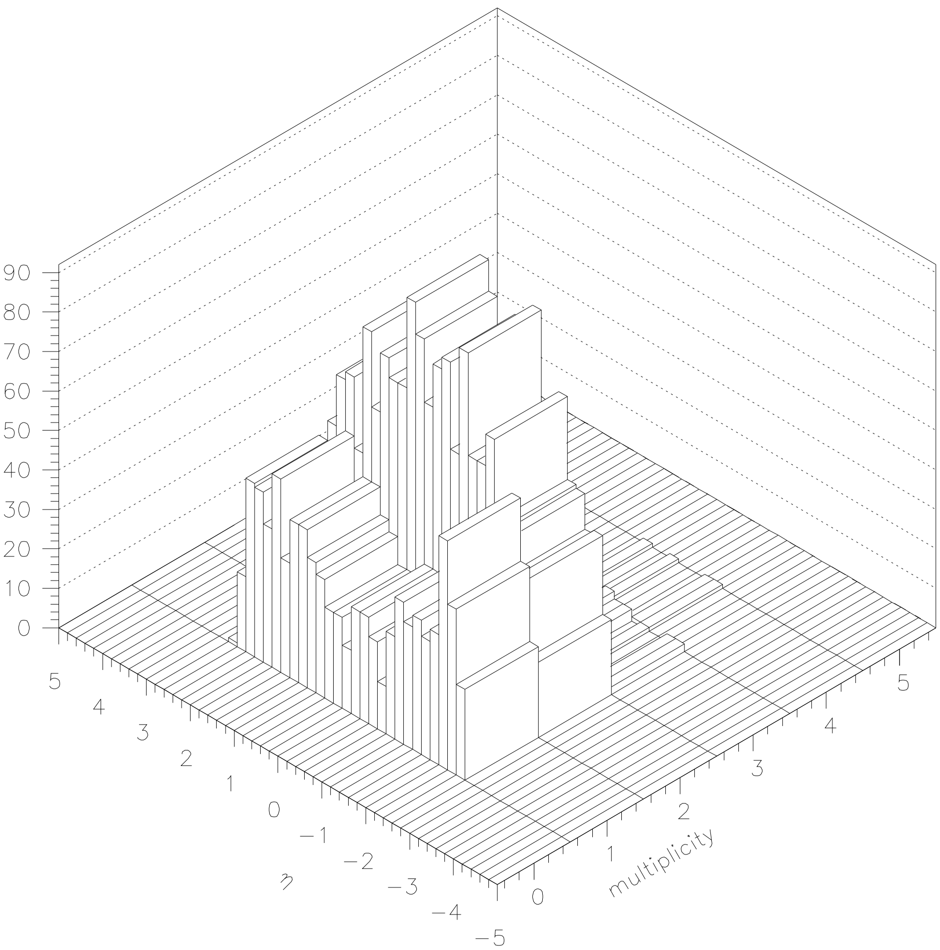

Figure 3.6: B-jet pseudorapidity η versus multiplicity before cuts.

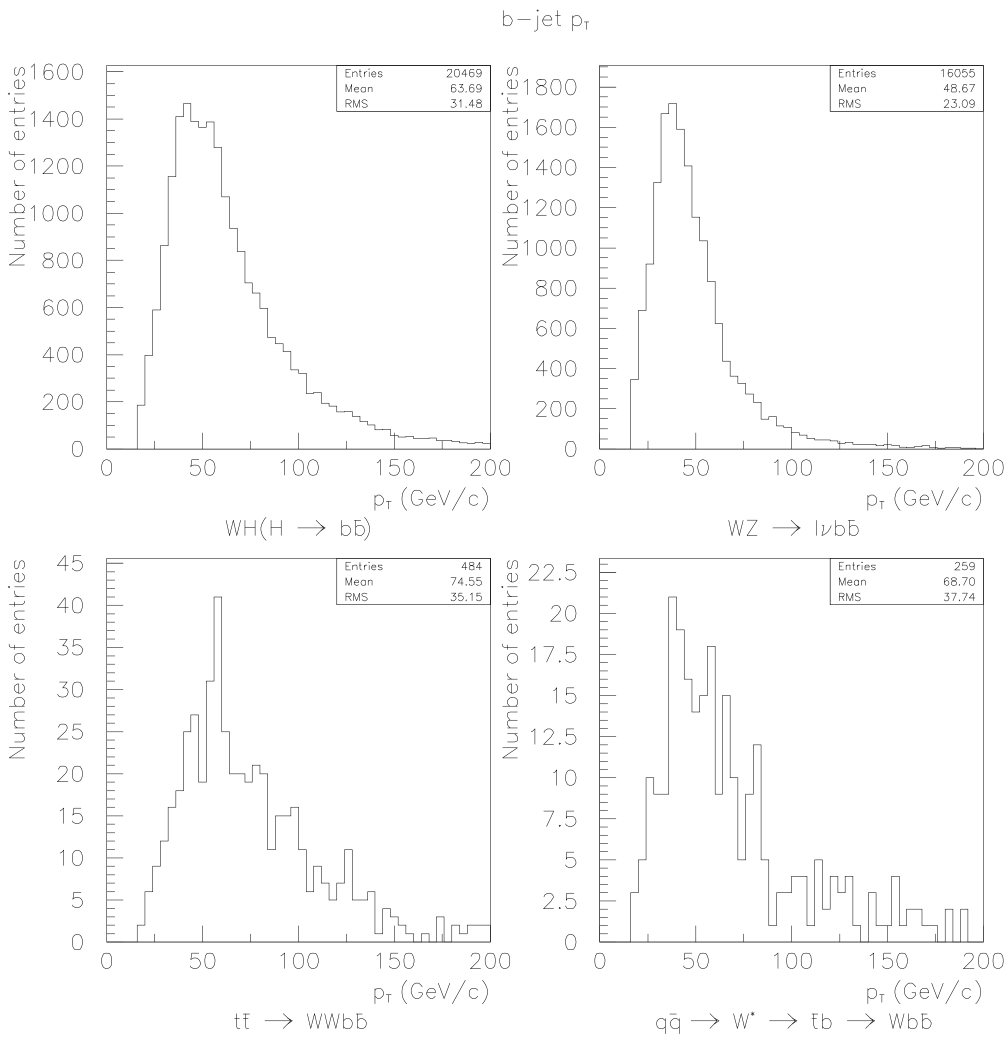

Figure 3.7: B-jet p_T after cuts.

$\eta - \phi$ space are different for the signal and WZ process. The lepton and b-jet seem to be more widely separated for the WZ background process. In a future analysis it might be interesting to examine the invariant mass of all possible pairs of leptons and b-jets.

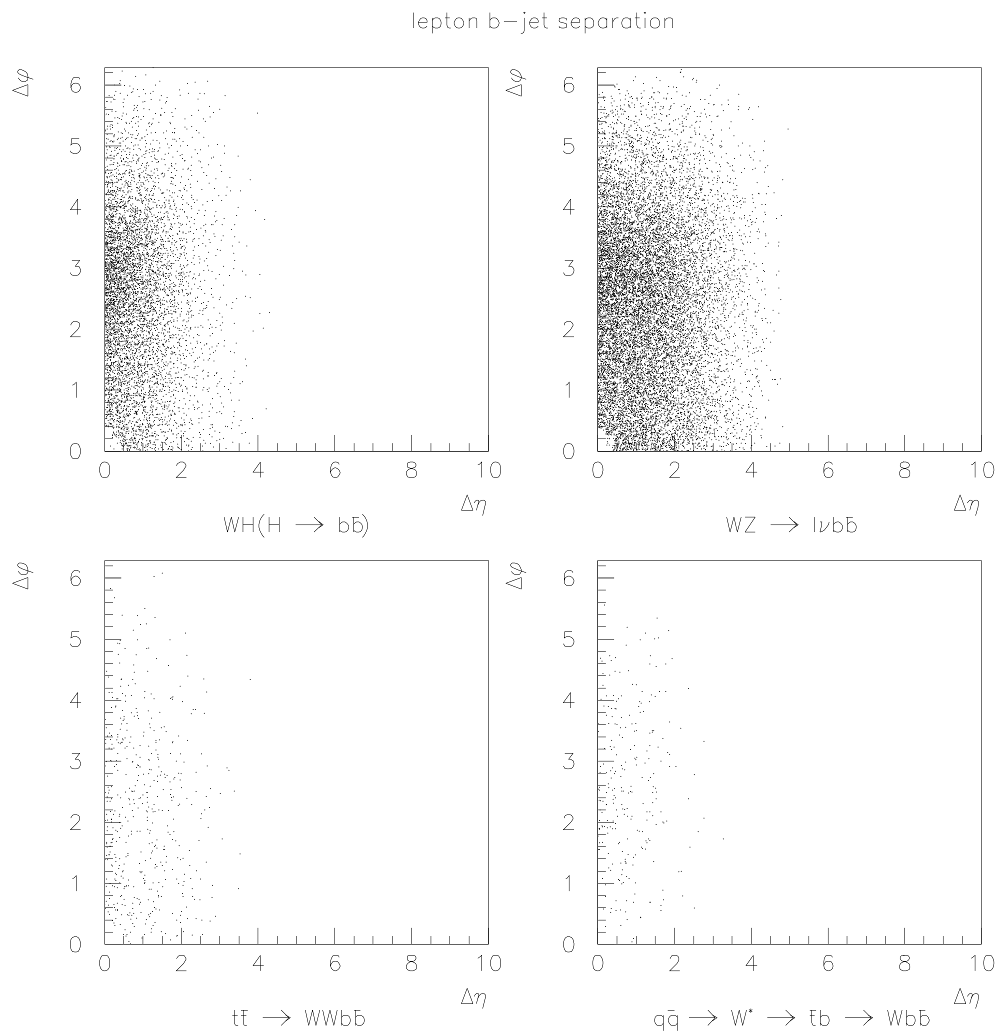

Figure 3.8: Lepton b-jet separation after cuts.

3.2 Conclusion

This was the first analysis of this type to be performed entirely in C++. In conclusion, the observation of a signal from $H \to b\bar{b}$ will be very difficult at the

LHC. Excellent b-tagging will be required. The results broadly agree with those published in the ATLAS TDR. Only a subset of the background processes could be generated reliably. The differences between the results in this study and those in the ATLAS TDR need to be understood. It is known from the ATLAS TDR that at least two backgrounds exist, that have not been successfully replicated for this study, that could have a detrimental effect on the feasibility of achieving a 5σ signal significance. It is not clear how these processes were generated for the ATLAS TDR. This analysis did not go beyond the analysis for the ATLAS TDR; it may be possible to design better cuts to enhance the signal. In any case, this study demonstrates that a first-attempt of an analysis written in C++ using Atlfast-Athena can produce results that are comparable to those produced from an analysis written in FORTRAN.

Bibliography

[1] S. L. Glashow, "Partial Symmetries Of Weak Interactions", Nucl. Phys. **22** (1961) 579.

[2] S. Weinberg, "A Model Of Leptons", Phys. Rev. Lett. **19** (1967) 1264.

[3] A. Salam, "Elementary Particle Theory", W. Svartholm, ed., Almqvist and Wiksell, Stockholm (1968) 367.

[4] D. E. Groom *et al.* [Particle Data Group Collaboration], "Review of particle physics", Eur. Phys. J. C **15** (2000) 1.

[5] L. Stodolsky, "The Speed Of Light And The Speed Of Neutrinos", Phys. Lett. B **201** (1988) 353.

[6] Y. Fukuda *et al.* [Super-Kamiokande Collaboration], "Evidence for oscillation of atmospheric neutrinos", Phys. Rev. Lett. **81** (1998) 1562 [hep-ex/9807003].

[7] G. 't Hooft, "Renormalization Of Massless Yang-Mills Fields", Nucl. Phys. B **33** (1971) 173.

[8] P. W. Higgs, "Broken Symmetries And The Masses Of Gauge Bosons", Phys. Rev. Lett. **13** (1964) 508.

[9] C. Caso *et al.* [Particle Data Group Collaboration], "Review of particle physics", Eur. Phys. J. C **3** (1998) 1.

[10] ATLAS Collaboration, ATLAS Detector and Physics Performance Technical Design Report, Volume 2, CERN/LHCC/99–15 (1999) 673.

[11] P. Teixeira-Dias, "The SM Higgs boson search at LEP: Combined results", hep-ex/0108002.

[12] D. Froidevaux and E. Richter-Was, "Is the channel $H \to b\bar{b}$ observable at LHC?", Z. Phys. C **67** (1995) 213.

[13] C. Peterson, D. Schlatter, I. Schmitt and P. Zerwas, "Scaling Violations In Inclusive e+ e- Annihilation Spectra", Phys. Rev. D **27** (1983) 105.

[14] A. Stange, W. Marciano and S. Willenbrock, "Associated production of Higgs and weak bosons, with $H \to b\bar{b}$, at hadron colliders", Phys. Rev. D **50** (1994) 4491 [hep-ph/9404247].

[15] T. Sjostrand, "High-energy physics event generation with PYTHIA 5.7 and JETSET 7.4", Comput. Phys. Commun. **82** (1994) 74.

[16] T. Sjostrand, P. Eden, C. Friberg, L. Lonnblad, G. Miu, S. Mrenna and E. Norrbin, "High-energy-physics event generation with PYTHIA 6.1", Comput. Phys. Commun. **135** (2001) 238 [hep-ph/0010017].